# Quantitative Double-Tracer Autoradiography with Tritium and Carbon-14 Using Imaging Plates: Application to Myocardial Metabolic Studies in Rats

Yuriko Yamane, Nobumasa Ishide, Yutaka Kagaya, Daiya Takeyama, Nobuyuki Shiba, Masanobu Chida, Yohei Sekiguchi, Tetsuji Nozaki, Tatsuo Ido and Kunio Shirato

*The First Department of Internal Medicine, School of Medicine and Cyclotron and Radioisotope Center, Tohoku University, Sendai, Japan*

A system for $^{3}H$- and $^{14}C$-labeled macroautoradiography was developed that is able to quantify the tissue radioactivity of two tracers using imaging plates. **Methods:** Discrimination between electrons emitted from $^{3}H$ and $^{14}C$ is possible on the basis of their different energy distributions. The general use imaging plate with a protective layer detects $^{14}C$ radioactivity, but it does not detect $^{3}H$ radioactivity which has a lower energy distribution than $^{14}C$. Recently, a $^{3}H$-sensitive imaging plate without a protective layer was developed. The $^{3}H$ distribution image is obtained by subtracting the UR image from the TR image. For quantification of the tissue radioactivity of $^{3}H$ and $^{14}C$, we obtained tissue equivalent values (Bq/mg) of commercially available $^{3}H$- and $^{14}C$-labeled graded standards using different dilutions of labeled heart paste and liquid scintillation counting. Using the $^{3}H$- and $^{14}C$-labeled graded standards, we confirmed the validity of the quantification of the $^{3}H$-autoradiographic intensity using this subtraction method. We applied this method to a rat model of acute myocardial ischemia to compare regional myocardial free fatty acid uptake determined by $\beta$-methyl[1-$^{14}C$]heptadecanoic acid to glucose uptake determined by 2-deoxy-D-[1-$^{3}H$]glucose. **Results:** Free fatty acid uptake was decreased sharply at the ischemic periphery where glucose uptake was preserved. **Conclusion:** This double-tracer autoradiography with $^{3}H$ and $^{14}C$ which has high sensitivity, a high spatial resolution of 50 $\mu$m and superior linearity with a wide dynamic range of $10^{4}$ to $10^{5}$ allows accurate quantification of the tissue radioactivity of the two radiopharmaceuticals.

**Key Words:** imaging plate; double-tracer autoradiography; tritium; carbon-14; myocardial glucose metabolism

**J Nucl Med 1995; 36:518–524**

Double-tracer autoradiography has been performed to investigate differences in the spatial distribution of two tracers in animals or organs. In previous studies, short-lived as well as long-lived radioisotopes were used for double labeling (*1–3*). The x-ray film is first exposed to the sections to depict the distribution of the shorter-lived radioisotope. Following a time interval equivalent to ten times the half-life of the shorter-lived radioisotope, the other x-ray film is exposed to the sections to determine the distribution of the longer-lived radioisotope (*1–3*). The use of double-tracer autoradiography with short-lived gamma- or positron-emitters and long-lived radioisotopes is becoming an important technique to provide the basis for clinical diagnostic studies using short-lived radioisotopes. Tissue equivalent standards of short-lived radioisotopes, however, are not commercially available. There is no assurance that the same optical density will be obtained by exposing an x-ray film to the same radiolabeled compound for the same duration. Therefore, tissue equivalent standards of short-lived radioisotopes need to be prepared, and need to be mounted with labeled tissue sections for each exposure. Tissue sections labeled with short-lived radioisotopes must be prepared as soon as possible after killing the animals, and the exposure must be performed before the decay of short-lived radioisotopes. Additionally, using the conventional x-ray film method, the relation between radioactivity and optical density is linear with a dynamic range of only $10^{2}$ (*2,4*).

A new system of computed radiography which eliminated the drawbacks of the conventional film method was developed in the last decade (*4–6*). In this system, imaging plates (IPs) coated with minute crystals of photostimulable phosphor are employed (*4–6*). Photostimulable phosphor is capable of storing the energy absorbed when excited by x-rays, electrons, ultraviolet rays or photons, and then emitting luminescence radiation corresponding to the absorbed energy when stimulated by visible or infrared radiation (photostimulated luminescence (PSL)) (*4–6*). The features of the imaging plate method are as follows (*4–6*). First, it has high sensitivity (several thousand times higher than that of the conventional x-ray film method) that allows

Received May 20, 1994; revision accepted Aug. 29, 1994.

For correspondence or reprints contact: Nobumasa Ishide, MD, Professor, The First Department of Internal Medicine, Tohoku University School of Medicine, 1-1 Seiryo-machi, Aoba-ku, Sendai 980-77, Japan.

lower injection doses of radiopharmaceuticals and shorter exposure time. Second, the dynamic range is $10^4$ to $10^5$ compared to about $10^2$ in the x-ray film method. Third, it has superior linearity over the entire range. Fourth, the spatial resolution is 50 $\mu$m.

IPs have been used for quantitative analysis in x-ray diffraction experiments (*7*) and autoradiography with $^{14}C$ (*8*). But electrons emitted from $^3H$ are not detected by the general use imaging plate (UR-IP) with a protective layer because of their low energy distribution. Recently, a tritium-sensitive imaging plate (TR-IP) without a protective layer has been developed, and it has been used with $^3H$-labeled radiopharmaceuticals and short-lived radioisotopes for autoradiographic studies (*9–11*). It has not been established, however, whether quantitative double-tracer autoradiography with two long-lived radioisotopes, $^3H$ and $^{14}C$, can be accomplished using both TR- and UR-IP. This method should have an apparent advantage because both $^3H$- and $^{14}C$-labeled graded standards are commercially available, and an accurate quantitative analysis for both radioisotopes would be possible.

In this study, using both TR- and UR-IP, we performed $^3H$- and $^{14}C$-labeled autoradiography for the first time in order to quantify the tissue radioactivity of the two tracers. The absolute tissue radioactivity of $^3H$ and $^{14}C$ was estimated using commercially available graded standards (*11,12*). We describe the new method of double-tracer autoradiography with two long-lived radioisotopes, $^3H$ and $^{14}C$, and provide the basis for quantitative analysis.

## MATERIALS AND METHODS

### Calibration for Tissue $^3H$ and $^{14}C$ Content

We used the computer-assisted image-processing system, BAS3000 (Fuji Photo Film, Tokyo, Japan) for the quantitative analysis of radioactivity. This system consists of an image reader, an image processor (a 32-bit workstation), a laser beam printer, a high-quality hard-copy printer (Pictrography, Fuji Photo Film, Tokyo, Japan) and an imaging plate eraser (*4–6*). The spatial resolution is 50 $\mu$m (*9*). The image data was recorded as the digitized values (PSL) of each pixel (50 $\mu$m × 50 $\mu$m) in the analyzing unit of this system (*9,11*).

In order to quantify tissue radioactivity, the autoradiographic intensities [(PSL-BG)/A] (BG, PSL of the background; A, area [$mm^2$]) must be converted into tissue $^3H$ and $^{14}C$ content [Bq/mg] using the calibration lines obtained from the $^3H$- and $^{14}C$-labeled graded standards. The $^3H$- and $^{14}C$-labeled graded standards (Amersham, Buckinghamshire, England) were calibrated according to their autoradiographic equivalence to the $^3H$ and $^{14}C$ content [Bq/mg wet weight] in 20-$\mu$m-thick heart sections (*11,12*). In four rats, 7.4 MBq of 2-deoxy-D-[1-$^3H$]glucose ($^3H$-DG), with specific activity 640 GBq/mmole, was injected intravenously and the hearts were removed 45 min postinjection. We made step-wedge heart paste standards as follows. Four $^3H$-labeled hearts were cut into pieces and homogenized together (paste A). We took a fraction of paste A, added a non-radioactive rat heart and homogenized them together (paste B). Pastes C and D were prepared by adding a non-radioactive heart to a fraction of pastes B and C, respectively. Each paste was frozen in dry ice, processed into 20-$\mu$m-thick sections and dried on a hot plate. The sections were placed along with the $^3H$-labeled graded standard in contact with TR-IP (Fuji Photo Film, Tokyo, Japan) for four weeks. We determined the autoradiographic intensities [(PSL-BG)/A] of each tissue paste and the polymers of the $^3H$-labeled graded standard. The $^3H$ radioactivity of the graded tissue paste [Bq/mg] was determined with a liquid scintillation counter (2050CA, Packard, Downers Grove, IL) using a small amount of the paste after measuring its wet weight. Using linear fitting, we obtained the following equation,

$$y = ax + b \qquad \text{Eq. 1}$$

where x is the autoradiographic intensity of the $^3H$-labeled heart paste [(PSL-BG)/A], and y is the tissue radioactivity [Bq/mg] determined by liquid scintillation counting. The tissue equivalent value of each polymer of the $^3H$-labeled graded standard was calculated using its autoradiographic intensity and Equation 1. The same procedure was performed to determine the tissue equivalent of each polymer of the $^{14}C$-labeled graded standard. In this series, 0.74 MBq of 2-deoxy-D-[U-$^{14}C$]glucose, with specific activity 10.434 GBq/mmole (New England Nuclear, Boston, Massachusetts), was injected. The tissue sections along with the $^{14}C$-labeled graded standard were placed in contact with UR-IP (Fuji Photo Film, Tokyo, Japan) for two weeks.

### Validation Study for Quantitative Double-Tracer Autoradiography with $^3H$ and $^{14}C$

For the quantitative double-tracer autoradiography, the tissue section along with the $^3H$- and $^{14}C$-labeled graded standards is placed in contact with TR-IP, and then along with the identical graded standards in contact with UR-IP for the same duration (Fig. 1). The image of $^{14}C$ is obtained using UR-IP. The image of $^3H$ is obtained by subtracting the UR image ($^{14}C$ image) from the TR image ($^3H$-plus-$^{14}C$ image). It is not certain, however, whether the $^{14}C$ intensity determined with UR-IP is identical to that determined with TR-IP. The $^{14}C$ intensity determined with UR-IP can be corrected in each experiment to agree with that determined with TR-IP, if the relation between the $^{14}C$ intensity determined with TR-IP and that determined with UR-IP is linear. To validate this, we placed the $^{14}C$-labeled graded standards (n = 29) in contact with TR-IP for two weeks, and with UR-IP for another two weeks. We determined the autoradiographic intensity [(PSL-BG)/A] of each polymer of the $^{14}C$-labeled graded standards placed in contact with TR- and UR-IP. Using the tissue equivalent values of the polymers of the $^{14}C$-labeled graded standard, the calibration lines of both the TR- and UR-images were obtained.

In order to confirm that electrons emitted from $^3H$ were not detectable with UR-IP, we exposed UR-IP to the $^3H$- and $^{14}C$-labeled graded standards for two weeks and TR-IP for another two weeks. On the color monitor display of the image-processing system, we traced the $^3H$- and $^{14}C$-labeled graded standards of the TR image on a transparent film attached to the display. Using the transparent film, the autoradiographic intensities of the $^3H$-labeled graded standards determined with UR-IP were obtained.

If the $^{14}C$ intensities are much higher than the $^3H$ intensities, the $^3H$ intensities obtained by this subtraction method might be scattered compared with the true $^3H$ intensities because of possible differences between the $^{14}C$ intensities determined with UR-IP and those determined with TR-IP. The $^3H$ intensities should be high enough to eliminate the artificial scattering of the calculated $^3H$ intensities. Using the $^{14}C$-labeled graded standards (n = 29), we obtained the differences between the $^{14}C$ intensities deter-

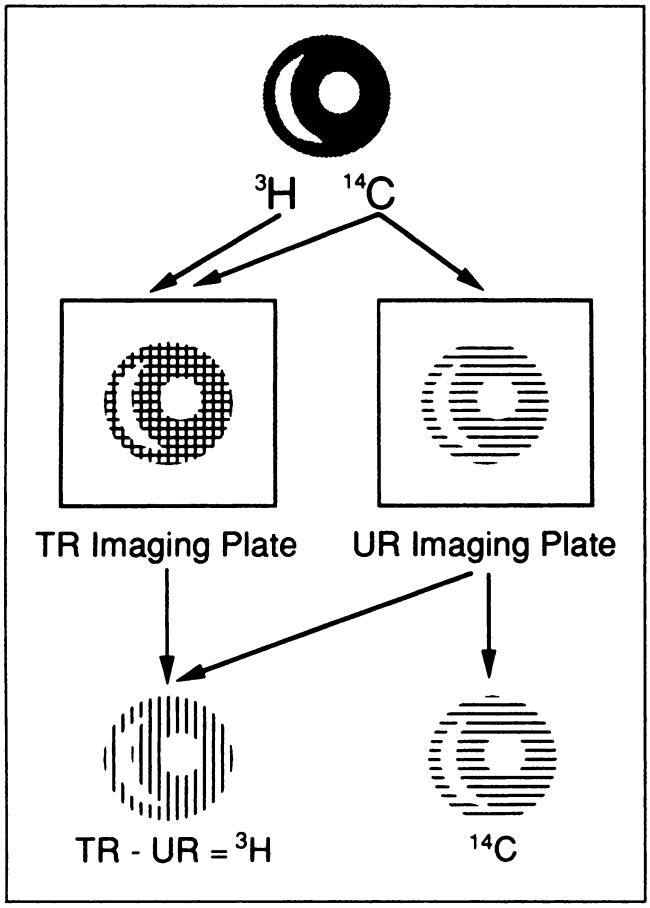


**FIGURE 1.** Principle of double-tracer autoradiography with $^3H$ and $^{14}C$ using imaging plates.

mined with TR-IP and the corrected $^{14}C$ intensities determined with UR-IP.

### Animal Studies

Male Wistar rats (260–356 g) were anesthetized with sodium pentobarbital (40 mg/kg i.p.). An arterial catheter (PE 50) was placed in the right common carotid artery for monitoring arterial blood pressure (model MPU 0.5, Nihon Koden, Tokyo, Japan) and for blood sampling. A venous catheter (PE 50) was inserted into the right jugular vein for the administration of radiopharmaceuticals. In the control group, after the insertion of an arterial and venous catheter, 3.7 MBq of 2-deoxy-D-[1-$^3$H]glucose ($^3$H-DG), with specific activity 640 GBq/mmole (Amersham, Buckinghamshire, England) (*13*), was injected intravenously for 30 sec to assess regional myocardial glucose uptake. Thirty seconds after the $^3$H-DG injection, 0.185 MBq of $\beta$-methyl[1-$^{14}$C]heptadecanoic acid ($^{14}$C-BMHDA), with specific activity 2.13 GBq/mmole (New England Nuclear, Boston, MA), dissolved in 0.2 ml of an aqueous solution of bovine serum albumin (*14*) was injected intravenously for 30 sec to assess regional myocardial free fatty acid uptake (*15*). Thirty minutes after the $^3$H-DG injection, the rats were killed with 0.3 ml of saturated KCl solution. The hearts were removed rapidly and frozen in dry ice. In the ischemia group, after left thoracotomy under artificial ventilation, a snare (6-0 nylon) was placed around the left coronary artery (LCA) at a point about 5 mm distal from its aortic ostium.

After the injection of 1 mg/kg of lidocaine to prevent ventricular arrhythmias, both suture ends were threaded through a polyethylene tube (PE 50), and the LCA was ligated (*16*). Just after the LCA ligation, 3.7 MBq of $^3$H-DG was injected intravenously for 30 sec, and 30 sec after that, 0.185 MBq of $^{14}$C-BMHDA was injected intravenously for 30 sec. Thirty minutes after the $^3$H-DG injection, the rats were injected intravenously with 2% methylene blue solution (0.5 ml) to demarcate the ischemic area by negative staining. Immediately afterwards, the rats were killed with 0.3 ml of saturated KCl solution. The hearts were removed rapidly and frozen in dry ice.

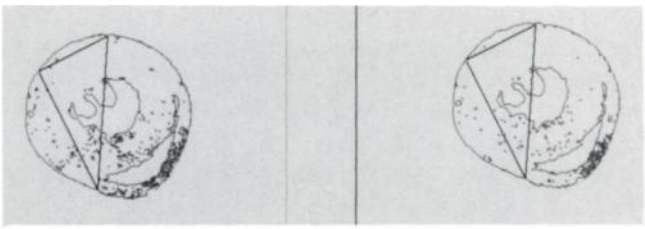

**FIGURE 2.** Subtraction method.

For autoradiography, 20-$\mu$m-thick frozen sections taken perpendicular to the long axis of the left ventricle were prepared using a cryomicrotome (975C-Histostat Microtome, American Optical, Buffalo, NY). The sections were picked up on plastic slips and dried on a hot plate at 60°C for more than 20 min. The sections along with the $^{14}$C- and $^3$H-labeled graded standards were placed in contact with TR-IP for two weeks, and with UR-IP for another two weeks.

The image of $^{14}$C-BMHDA was obtained using UR-IP, and the image of $^3$H-DG was obtained by subtracting the UR image from the TR image. Details of the subtraction method are as follows (Fig. 2). First, TR-and UR-outline images are drawn using an edge-detecting program of an image processor. Second, three points are selected as landmarks on the same sites of the TR-and UR-outline images. Third, two images are superimposed using the landmarks. Finally, the $^3$H image is obtained by subtracting the UR image from the TR image.

We calculated regional myocardial $^{14}$C-BMHDA uptake and $^3$H-DG uptake as follows. The $^{14}$C calibration lines of the TR image (Eq. 2) and the UR image (Eq. 3) were obtained.

$$y = ax + b \qquad \text{Eq. 2}$$

$$y = a'x + b' \qquad \text{Eq. 3}$$

where x is the autoradiographic intensity of the $^{14}$C-labeled graded standard [(PSL-BG)/A], and y is the tissue equivalent [Bq/mg]. The $^3$H calibration line of the TR image was obtained.

$$y = cx + d \qquad \text{Eq. 4}$$

where x is the autoradiographic intensity of the $^3$H-labeled graded standard [(PSL-BG)/A], and y is the tissue equivalent [Bq/mg]. Regional myocardial $^{14}$C-BMHDA uptake [Bq/mg] was obtained from the UR image intensity and Equation 3.

The $^3$H intensity [(PSL-BG)/A] of the TR image was obtained.

$$(^3\text{H intensity}) = \text{TR} - \text{URcorrected}$$

$$= \text{TR} - \text{UR} \times (a'/a) \qquad \text{Eq. 5}$$

$$\text{URcorrected} = \text{UR} \times (a'/a) \qquad \text{Eq. 6}$$

where TR is the TR image intensity, URcorrected is the corrected UR image intensity, UR is the UR image intensity and a and a′ are

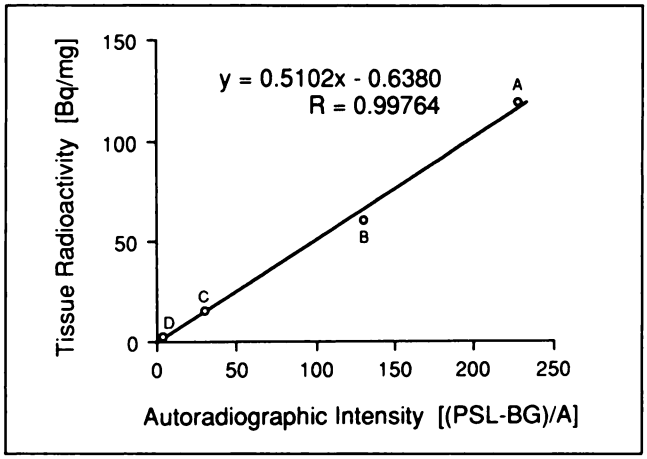


**FIGURE 3.** Relation between autoradiographic intensity and tissue radioactivity of $^{3}H$-labeled heart paste.

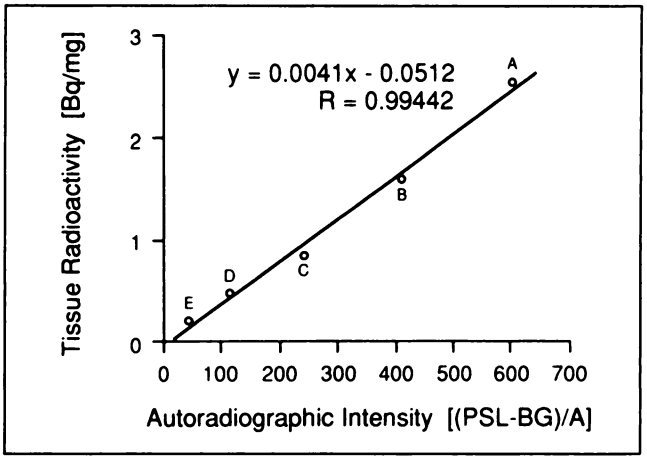


**FIGURE 4.** Relation between autoradiographic intensity and tissue radioactivity of $^{14}C$-labeled heart paste.

the slopes of the $^{14}C$ calibration lines of the TR and the UR image, respectively.

Regional myocardial $^{3}H$-DG uptake [Bq/mg] was obtained from Equations 5 and 4.

In the ischemia group, the heart sections were photographed, and the transparencies were projected on a rear-projection theater (Neo Vision, Sugiura Lab., Tokyo, Japan). We traced the myocardial outline and the normally perfused area stained by the dye on a transparent film. Data are presented as mean ± s.d.

The purpose and nature of this study were approved by the Committee of Animal Experiments in the Cyclotron and Radioisotope Center of Tohoku University.

**TABLE 1**
Tissue Equivalent of $^{3}H$-Labeled Graded Standard

| Level | Tissue equivalent (Bq/mg "wet weight") | Polymer activity* (Bq/mg) |
|---|---|---|
| Higher Activity Range (RPA 506†) | | |
| 1 | 625.6 | 3932.4 |
| 2 | 390.9 | 2299.6 |
| 3 | 246.8 | 1425.6 |
| 4 | 148.5 | 852.1 |
| 5 | 93.6 | 521.0 |
| 6 | 61.1 | 333.7 |
| 7 | 35.5 | 185.7 |
| 8 | 22.1 | 111.0 |
| Lower Activity Range (RPA 507†) | | |
| 1′ | 117.8 | 589.8 |
| 2′ | 57.1 | 303.4 |
| 3′ | 37.2 | 195.7 |
| 4′ | 13.9 | 76.2 |
| 5′ | 7.85 | 39.2 |
| 6′ | 3.07 | 19.0 |
| 7′ | 0.98 | 9.47 |

*From the Amersham catalog.
†Amersham code number.

## RESULTS

### Calibration for Tissue $^{3}H$ and $^{14}C$ Content

The relationship between autoradiographic intensity [(PSL-BG)/A] of the $^{3}H$-labeled heart paste and its tissue radioactivity [Bq/mg] determined by liquid scintillation counting is shown in Figure 3. Linear fitting was used to obtain the equation: $y = 0.5102x - 0.6380$ ($R = 0.99764$) (x, autoradiographic intensity [(PSL-BG)/A]; y, tissue radioactivity [Bq/mg]). The tissue equivalent values [Bq/mg] of the polymers of the $^{3}H$-labeled graded standard were calculated with this equation (Table 1).

The relationship between autoradiographic intensity [(PSL-BG)/A] of the $^{14}C$-labeled heart paste and its tissue radioactivity [Bq/mg] determined by liquid scintillation counting is shown in Figure 4. Linear fitting was used to obtain the equation: $y = 0.0041x - 0.0512$ ($R = 0.99442$). Again, tissue equivalent values [Bq/mg] of the polymers of the $^{14}C$-labeled graded standard were calculated with this equation (Table 2).

### Validation Study for Quantitative Double-Tracer Autoradiography with $^{3}H$ and $^{14}C$

From the TR image of the $^{14}C$-labeled graded standard ($n = 29$) placed in contact with TR-IP for 2 wk, we obtained the calibration line, $y = ax + b$ (x, autoradiographic intensity [(PSL-BG)/A]; y, tissue equivalent [Bq/mg]). From the UR image of the same $^{14}C$-labeled graded standard, we obtained the other calibration line, $y = a'x + b'$. The values of a, a′, b and b′ were $0.0056 \pm 0.0007$, $0.0055 \pm 0.0005$, $-0.0344 \pm 0.0419$ and $-0.0315 \pm 0.0404$, respectively. The value of a′/a obtained from the same $^{14}C$-labeled graded standard was $1.0018 \pm 0.0854$ (Table 3). The correlation coefficients of the $^{14}C$ calibration lines of the TR and UR images were $0.99994 \pm 0.00007$ and $0.99992 \pm 0.00013$, respectively.

Using the same $^{14}C$-labeled graded standard, the $^{14}C$ intensity determined with UR-IP was not always equal to that determined with TR-IP as shown in Figure 5. But the

**TABLE 2**
Tissue Equivalent of $^{14}$C-Labeled Graded Standard

| Level | Tissue equivalent (Bq/mg "wet weight") | Polymer activity* (Bq/mg) |
|---|---|---|
| Higher Activity Range (RPA 504L†) | | |
| 2 | 15.30 | 26.20 |
| 3 | 11.38 | 19.61 |
| 4 | 7.63 | 13.17 |
| 5 | 4.96 | 8.70 |
| 6 | 2.54 | 4.51 |
| 7 | 1.23 | 2.22 |
| 8 | 0.58 | 1.15 |
| Lower Activity Range (RPA 511L†) | | |
| 1′ | 1.94 | 3.85 |
| 2′ | 0.93 | 1.89 |
| 3′ | 0.45 | 0.95 |
| 4′ | 0.15 | 0.38 |
| 5′ | 0.03 | 0.19 |

*From the Amersham catalog.
†Amersham code number.

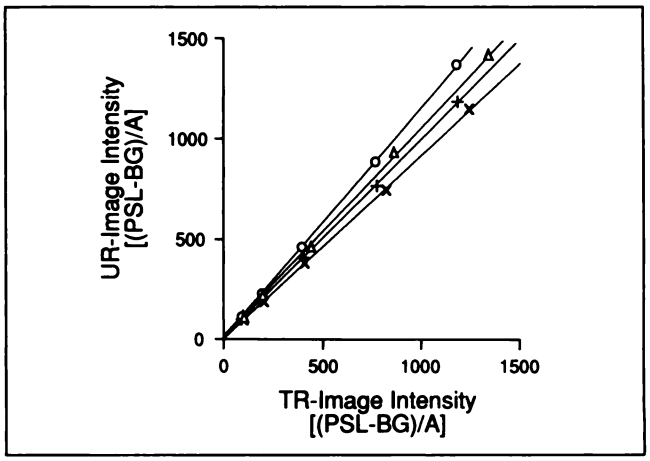


**FIGURE 5.** Relationship between autoradiographic intensity of $^{14}$C-labeled graded standards determined with TR-IP and that determined with UR-IP. The A of the $^{14}$C-labeled graded standards No. 6 (x), No. 9 (△), No. 11 (+) and No. 21 (○) were 0.9312, 1.0657, 1.0028 and 1.1679, respectively. All data obtained from the $^{14}$C-labeled graded standards (n = 29) are shown in Table 3.

relation between the $^{14}$C intensity determined with TR- and UR-IP was linear. The A, B and the correlation coefficient of the linearly fitted line (UR = A × TR + B) were 1.0103 ± 0.0928, −0.3157 ± 2.9348 and 0.99996 ± 0.00007 (n = 29), respectively (Table 3). After correcting the $^{14}$C intensities determined with UR-IP using Equation 6, the A′, B′ and the correlation coefficient of the linearly fitted line (URcorrected = A′ × TR + B′) were 0.9998 ± 0.0008, −0.3162 ± 3.0576 and 0.99996 ± 0.00007 (n = 29), respectively (Fig. 6 and Table 3).

The $^{3}$H-standard polymers (tissue equivalent ≤117.8 Bq/mg) placed in contact with UR-IP for two weeks were not visualized, and their autoradiographic intensities did not exceed the background level. The $^{3}$H-standard polymers with higher activity (tissue equivalent ≥148.5 Bq/mg) were slightly visualized with UR-IP, but the $^{3}$H intensities determined with UR-IP were less than 1% of that determined with TR-IP.

Using the $^{14}$C-standard polymer (tissue equivalent = 0.58 Bq/mg, n = 28), the $^{14}$C intensity determined with TR-IP, that determined with UR-IP, and the corrected $^{14}$C intensity determined with UR-IP were 114.4 ± 16.6, 113.9 ± 11.9 and 114.4 ± 17.2 (PSL-BG)/A, respectively. The difference between the $^{14}$C intensity determined with TR-IP and the corrected $^{14}$C intensity determined with UR-IP was 0.0 ± 2.2 (PSL-BG)/A. Using the other $^{14}$C-standard polymer (tissue equivalent = 1.23 Bq/mg, n = 29), the $^{14}$C intensity determined with TR-IP, $^{14}$C intensity determined with UR-IP and the corrected $^{14}$C intensity determined with UR-IP were 227.5 ± 33.9, 226.4 ± 24.0 and 227.8 ± 33.9 (PSL-BG)/A, respectively. The difference between the $^{14}$C intensity determined with TR-IP and the corrected $^{14}$C intensity determined with UR-IP was 0.3 ± 3.0 (PSL-BG)/A. In order to keep the standard deviation of the difference between the $^{14}$C intensity determined with TR-IP and the corrected $^{14}$C intensity determined with UR-IP below 5% of the $^{3}$H intensities, the $^{3}$H intensities combined with the $^{14}$C intensities of 114 and 228 (PSL-BG)/A needed to be higher than 44 and 60 (PSL-BG)/A, respectively.

### Animal Studies

Figure 7 shows representative autoradiograms from the hearts of rats in the control group (upper panels) and in the ischemia group (lower panels). In the control group, left ventricular $^{14}$C-BMHDA uptake and $^{3}$H-DG uptake was almost homogenous. In the ischemia group, however, an area with a reduced concentration of $^{14}$C-BMHDA appeared in the anterior, lateral and posterior walls of the left ventricle (lower middle panel). The area with a reduced

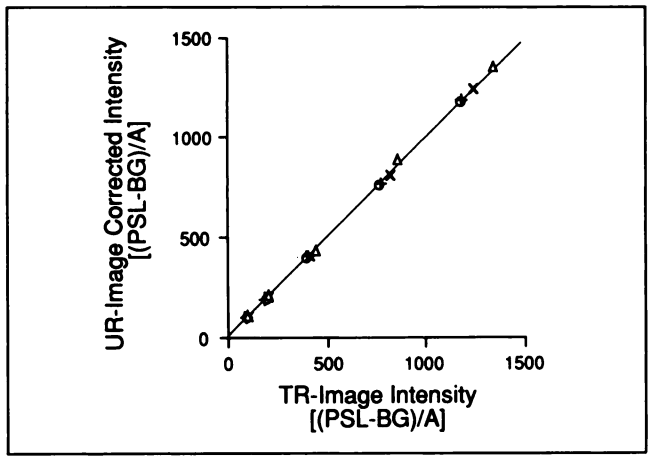


**FIGURE 6.** Correction of autoradiographic intensity of $^{14}$C-labeled graded standards determined with UR-IP in order to agree with that determined with TR-IP. The A′ of the $^{14}$C-labeled graded standards No. 6 (x), No. 9 (△), No. 11 (+) and No. 21 (○) were 0.9999, 0.9998, 1.0000 and 1.0000, respectively. All data obtained from the $^{14}$C-labeled graded standards (n = 29) are shown in Table 3.

**TABLE 3**
Accurate Correction of $^{14}C$ Intensity Determined with UR-IP

| No. | a'/a | A | A' |
|---|---|---|---|
| 1 | 0.9073 | 1.1022 | 1.0000 |
| 2 | 0.9476 | 1.0554 | 1.0000 |
| 3 | 0.9467 | 1.0563 | 1.0000 |
| 4 | 1.0446 | 0.9573 | 0.9999 |
| 5 | 1.0081 | 0.9919 | 1.0000 |
| 6 | 1.0738 | 0.9312 | 0.9999 |
| 7 | 0.9376 | 1.0658 | 0.9992 |
| 8 | 0.9840 | 1.1620 | 1.0000 |
| 9 | 0.9381 | 1.0657 | 0.9998 |
| 10 | 0.9210 | 1.0858 | 1.0000 |
| 11 | 0.9972 | 1.0028 | 1.0000 |
| 12 | 1.0146 | 0.9856 | 1.0000 |
| 13 | 0.9978 | 1.0022 | 1.0000 |
| 14 | 1.0580 | 0.9412 | 0.9958 |
| 15 | 1.0967 | 0.9117 | 0.9999 |
| 16 | 1.0721 | 0.9327 | 1.0000 |
| 17 | 1.0349 | 0.9662 | 1.0000 |
| 18 | 1.1093 | 0.9015 | 1.0000 |
| 19 | 1.1010 | 0.9082 | 1.0000 |
| 20 | 1.1044 | 0.9055 | 1.0000 |
| 21 | 0.8562 | 1.1679 | 1.0000 |
| 22 | 0.8743 | 1.1437 | 0.9999 |
| 23 | 1.0768 | 0.9287 | 1.0000 |
| 24 | 1.0970 | 0.9115 | 0.9999 |
| 25 | 1.0908 | 0.9167 | 1.0000 |
| 26 | 1.1169 | 0.8953 | 1.0000 |
| 27 | 0.8795 | 1.1370 | 1.0000 |
| 28 | 0.8923 | 1.1206 | 1.0000 |
| 29 | 0.8726 | 1.1460 | 1.0000 |
| mean | 1.0018 | 1.0103 | 0.9998 |
| ±SD | ±0.0854 | ±0.0928 | ±0.0008 |

concentration of $^{14}C$-BMHDA agreed with the ischemic area visually determined by negative staining of the dye (M- in left panel of Fig. 8). Tritium-DG uptake was preserved at the lateral borders, subendocardium and subepicardium within the ischemic area (lower right panel of Fig. 7).

We quantified the regional myocardial $^{14}C$-BMHDA uptake and $^{3}H$-DG uptake in the normally perfused area (Norm), at the lateral borders in the ischemic area (Bord) and at the center of the ischemic area (Cent) as shown in the right panel of Figure 8. The regional myocardial $^{14}C$-BMHDA uptake in Norm, Bord and Cent were 2.02 (100%), 0.46 (23%) and 0.00 Bq/mg (0% of that in Norm), respectively. The regional myocardial $^{3}H$-DG uptake in Norm, Bord and Cent were 112 (100%), 86 (77%) and 4 Bq/mg (4%), respectively.

## DISCUSSION

The scanner was set to obtain the same autoradiographic intensity when TR- and UR-IP are exposed to the same $^{14}C$-labeled compound for the same short duration. In this study with two weeks exposure, however, the ratios of the intensities of the $^{14}C$-labeled polymers determined with UR-IP to that determined with TR-IP was 0.88–1.17, 1.01 ± 0.09 (n = 232) (data not shown). There might be

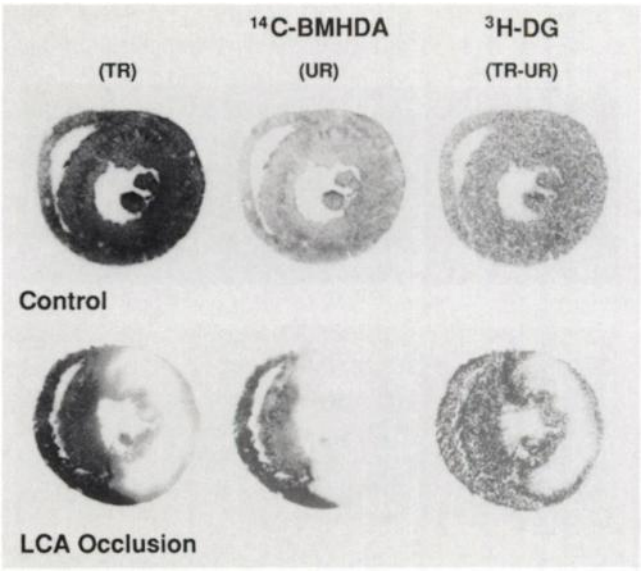


**FIGURE 7.** Double-tracer autoradiograms labeled with $^{14}C$-BMHDA and $^{3}H$-DG in rat hearts.

some factors which caused differences between the $^{14}C$ intensity determined with TR-IP and that determined with UR-IP. First, the differences of the exposure time between TR- and UR-IP were less than 2% of two weeks. Second, the fading effect of the energy stored in IP is assumed to occur during the two weeks' exposure at room temperature. The fading effect in the TR-IP might be different from that in the UR-IP. Third, the condition of the scanner, especially that of the photomultiplier tube, might also have been different in each scanning. Nevertheless, we could cancel the differences between the $^{14}C$ intensity determined with TR-IP and that determined with UR-IP by correcting with the calibration lines obtained from the $^{14}C$-labeled graded standards placed in contact with TR- and UR-IP in each experiment. In the present study, the superior linearity of the imaging plate method was demonstrated, because the correlation coefficients of the $^{14}C$ calibration lines of the TR- and UR images were 0.99994 ± 0.00007 and 0.99992 ± 0.00013, respectively. Therefore, an

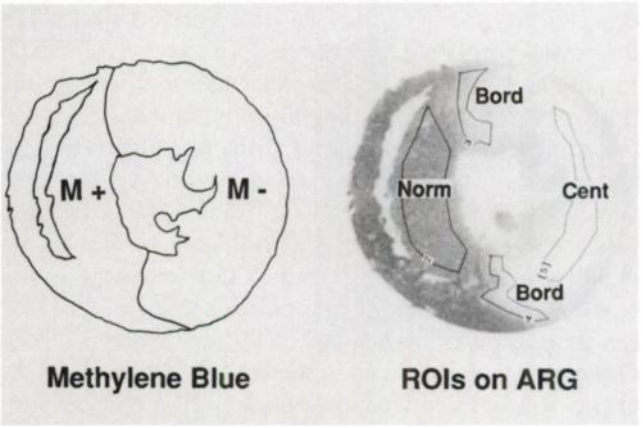


**FIGURE 8.** Trace of heart section stained by methylene blue (left panel) and regions of interest (ROIs) placed on autoradiogram (ARG) of the same heart section (right panel).

accurate correction of the $^{14}C$ intensity determined with TR and UR-IP was performed using the calibration lines obtained from the $^{14}C$-labeled graded standards.

In this double-tracer autoradiography with $^{3}H$ and $^{14}C$, the $^{14}C$ distribution image is obtained using UR-IP which does not detect the radioactivity of $^{3}H$. On the other hand, the $^{3}H$ distribution image is obtained by subtracting the $^{14}C$ distribution image (UR image) from the $^{3}H$- plus -$^{14}C$ distribution image (TR image). A negligible error remains in measuring the $^{14}C$ intensity with TR- and UR-IP even after correcting with the $^{14}C$ calibration lines, because the decay of radioisotopes is subject to the laws of probability. The $^{3}H$ intensity needs to be high enough to eliminate the artificial scattering by the difference between the $^{14}C$ intensity determined with TR-IP and the corrected $^{14}C$ intensity determined with UR-IP. We showed that the $^{3}H$ intensity needed to be more than 30 to 40% of the $^{14}C$ intensity. In order to minimize the noise of the $^{3}H$-image, however, the $^{3}H$ intensity should be equal or higher than the $^{14}C$ intensity. In this study, the $^{3}H$-tissue radioactivity [Bq/mg] needed to be about 200 times higher than the $^{14}C$-tissue radioactivity to obtain the same autoradiographic intensity. Tritiated radiopharmaceuticals have higher specific activity [Bq/mole] compared with $^{14}C$-labeled ones. It might be possible to use much larger radioactivity of $^{3}H$ compared with $^{14}C$.

In this study, the spatial distribution of $^{3}H$-DG uptake in rat hearts was visualized clearly using TR- and UR-IP. The spill-over effects of radioactivity from ventricular walls to ventricular cavities and surroundings of the hearts were more prominent in TR images compared with UR images. Therefore, artificial intensities of ventricular cavities and surroundings of the hearts might be enhanced in the $^{3}H$-subtraction images.

In previous studies, it was reported that free fatty acids were the major fuels of the myocardium in the fasting state (*17,18*). In mild ischemia, however, glucose extraction increased concurrently with the formation of lactate, showing that mild ischemia could enhance glycolysis (*17–20*). In the present study, glucose uptake at the lateral borders in the ischemic area was 77% of that in the normally perfused area, but free fatty acid uptake was decreased to 23% of that in the normally perfused area. Vascular territories in rats are considered to be sharply demarcated without native collaterals (*21*). The present study, however, showed the existence of a border zone at the ischemic periphery where blood flow was decreased (but preserved to some degree), and glucose uptake was maintained compared with free fatty acid uptake. This is in agreement with our preliminary study using $^{14}C$ and $^{11}C$ (short-lived positron emitter) (*22*). Free fatty acid uptake is decreased in mild ischemia because $\beta$-oxidation of fatty acid is inhibited (*17*). Glucose might be taken up instead of free fatty acids as the energy source in mild ischemia.

Double-tracer autoradiography with $^{3}H$ and $^{14}C$ using imaging plates permits accurate quantification of the tissue radioactivity of two radiopharmaceuticals. It has the potential to become a very useful tool in the quantitative analysis of relationships between two kinds of biological information.

## REFERENCES


1. Yonekura Y, Brill AB, Som P, Bennett GW, Fand I. Quantitative autoradiography with radiopharmaceuticals, Part 1: Digital film-analysis system by videodensitometry: concise communication. *J Nucl Med* 1983;24:231–237.
2. Som P, Yonekura Y, Oster ZH, et al. Quantitative autoradiography with radiopharmaceuticals, part 2: applications in radiopharmaceutical research: concise communication. *J Nucl Med* 1983;24:238–244.
3. Kubota K, Som P, Oster ZH, et al. Detection of cardiomyopathy in an animal model using quantitative autoradiography. *J Nucl Med* 1988;29: 1697–1703.
4. Hamaoka T. Autoradiography of new era replacing traditional x-ray film: bio-imaging analyzer BAS2000. *Cell Technology* 1990;9:456–462.
5. Sonoda M, Takano M, Miyahara J, Kato H. Computed radiography utilizing scanning laser stimulated luminescence. *Radiology* 1983;148:833–838.
6. Amemiya Y, Miyahara J. Imaging plate illuminates many fields. *Nature* 1988;336:89–90.
7. Amemiya Y, Wakabayashi K, Tanaka H, Ueno Y, Miyahara J. Laser-stimulated luminescence used to measure x-ray diffraction of a contracting striated muscle. *Science* 1987;237:164–168.
8. Hori T, Tanaka S, Nishiyama M, et al. Distribution of intrathecally administered ACNU in mongrel dogs: pharmacokinetics and quantitative autoradiographic study. *Surg Neurol* 1993;40:183–195.
9. Yanai K, Ryu JH, Watanabe T, Iwata R, Ido T. Receptor autoradiography with $^{11}C$ and [$^{3}H$]-labelled ligands visualized by imaging plates. *NeuroReport* 1992;3:961–964.
10. Ryu JH, Yanai K, Iwata R, Ido T, Watanabe T. Heterogeneous distributions of histamine H3, dopamine D1 and D2 receptors in rat brain. *NeuroReport* 1994;5:621–624.
11. Nakagawa Y, Yanai K, Ryu JH, Kiyosawa M, Tamai M, Watanabe T. Marked increase in [$^{3}H$](R)$\alpha$-methylhistamine binding in the superior colliculus of visually deprived rats after unilateral enucleation. *Brain Res* 1994; 643:74–80.
12. Reivich M, Jehle J, Sokoloff L, Kety SS. Measurement of regional cerebral blood flow with antipyrine-$^{14}C$ in awake cats. *J Appl Physiol* 1969;27:296–300.
13. Sokoloff L, Reivich M, Kennedy C, et al. The [$^{14}C$]deoxyglucose method for the measurement of local cerebral glucose utilization: theory, procedure, and normal values in the conscious and anesthetized albino rat. *J Neurochem* 1977;28:897–916.
14. Hoffman EJ, Phelps ME, Weiss ES, et al. Transaxial tomographic imaging of canine myocardium with $^{11}C$-palmitic acid. *J Nucl Med* 1977;18:57–61.
15. Abendschein DR, Fox KAA, Dieter Ambos H, Sobel BE, Bergmann SR. Metabolism of beta-methyl[1-$^{11}C$]heptadecanoic acid in canine myocardium. *Nucl Med Biol* 1987;14:579–585.
16. Sievers RE, Schmiedl U, Wolfe CL, et al. A model of acute regional myocardial ischemia and reperfusion in the rat. *Magn Reson Med* 1989;10: 172–181.
17. Liedtke AJ. Alterations of carbohydrate and lipid metabolism in the acutely ischemic heart. *Prog Cardiovasc Dis* 1981;23:321–336.
18. Camici P, Ferrannini E, Opie LH. Myocardial metabolism in ischemic heart disease: basic principles and application to imaging by positron emission tomography. *Prog Cardiovasc Dis* 1989;32:217–238.
19. Rovetto MJ, Lamberton WF, Neely JR. Mechanisms of glycolytic inhibition in ischemic rat hearts. *Circ Res* 1975;37:742–751.
20. Opie LH. Effects of regional ischemia on metabolism of glucose and fatty acids: relative rates of aerobic and anaerobic energy production during myocardial infarction and comparison with effects of anoxia. *Circ Res* 1976;38 Suppl. 1:I-52–68.
21. Schaper W. Experimental infarcts and the microcirculation. In: Hearse DJ, Yellon DM, eds. *Therapeutic approaches to myocardial infarct size limitation.* New York: Raven Press; 1984:79–90.
22. Kanno Y, Kagaya Y, Ishide N, et al. Alteration in myocardial substrate uptake forms lateral metabolic border zone during regional ischemia in rats. *Circulation* 1986;74 (suppl II):II–352.